A new highly sensitive cryogenic luminescent thermometer MOF built with pyromellitic acid

Amiaud T., Jubera V., Serier-Brault H.[*]

1. Experimental procedures

1.1. Synthesis of materials

{[Eu$_2$(H$_2$Btec)(Btec)(H$_2$O)$_2$]·4H$_2$O}$_n$: H$_4$Btec (381.2 mg, 1.50 mmol) and Eu(NO$_3$)$_3$·6H$_2$O (334.5 mg, 0.75 mmol) were dissolved in 15 mL distilled water. The mixture was placed in a sealed 23 mL Teflon lined stainless vessel, which was heated at 130°C for 3 days under autogenous pressure and cooled down to room temperature. The as-obtained white powder was finally recovered by filtration, and washed with EtOH. Yield: 0.125 g (**36 %**). Anal. Calcd. for Eu$_2$C$_{20}$O$_{22}$H$_{18}$ (%) : C, 26.3 ; H, 2.0. Exp: C, 26.3; H, 1.7. IR (KBr pellet, cm^{-1}): 3506 (vs), 3412 (vs), 2797 (w), 2650 (w), 2515 (m), 1657 (vs), 1612 (s), 1580 (vs), 1557 (s), 1499 (s), 1429 (s), 1389 (vs), 1294 (m), 1271 (m), 1124 (m), 883 (m), 837 (s), 658 (s), 590 (s), 521 (s), 444 (m), 411 (m).

{[Tb$_2$(H$_2$Btec)(Btec)(H$_2$O)$_2$]·4H$_2$O}$_n$: H$_4$Btec (114.4 mg, 0.45 mmol) and TbCl$_3$·6H$_2$O (168.0 mg, 0.45 mmol) were dissolved in 15 mL distilled water. The mixture was placed in a sealed 23 mL Teflon lined stainless vessel, which was heated at 130°C for 3 days under autogenous pressure and cooled down to room temperature. Small transparent crystals were finally recovered by filtration, and washed with EtOH. Yield: 0.083 g (**40%**). Anal. Calcd. for pour Tb$_2$C$_{20}$O$_{22}$H$_{18}$ (%): C, 25.9 ; H, 2.0. Exp: C, 25.9; H, 1.8. IR (KBr pellet, cm^{-1}): 3504 (vs), 3412 (vs), 2797 (w), 2648 (w), 2513 (m), 1657 (vs), 1612 (s), 1580 (vs), 1556 (s), 1499 (s), 1429 (s), 1389 (vs), 1294 (m), 1271 (m), 1124 (m), 881 (m), 837 (s), 658 (s), 590 (s), 521 (s), 442 (m), 409 (m).

{[Gd$_2$(H$_2$Btec)(Btec)(H$_2$O)$_2$]·4H$_2$O}$_n$: H$_4$Btec (381.2 mg, 1.50 mmol) and Gd(NO$_3$)$_3$·6H$_2$O (338.5 mg, 0.75 mmol) were dissolved in 15 mL distilled water. The mixture was placed in a sealed 23 mL Teflon lined stainless vessel, which was heated at 130°C for 3 days under autogenous pressure and cooled down to room temperature. The as-obtained white powder was finally recovered by filtration, and washed with EtOH. Yield: 0.112 g (**32 %**). Anal. Calcd. for Gd$_2$C$_{20}$O$_{22}$H$_{18}$ (%): C, 26.0 ; H, 2.0. Exp: C, 26.0 ; H, 1.8. IR (KBr pellet, cm^{-1}): 3508 (vs), 3414 (vs), 2799 (w), 2650 (w), 2515 (m), 1659 (vs), 1612 (s), 1580 (vs), 1556 (s), 1499 (s), 1429 (s), 1389 (vs), 1294 (m), 1269 (m), 1124 (m), 881 (m), 837 (s), 658 (s), 590 (s), 521 (s), 444 (m), 409 (m).

{[Tb$_{2-x}$Eu$_x$(H$_2$Btec)(Btec)(H$_2$O)$_2$]·4H$_2$O}$_n$: H$_4$Btec (114.4 mg, 0.45 mmol) and an appropriate mixture of TbCl$_3$·6H$_2$O and Eu(NO$_3$)$_3$·6H$_2$O were dissolved in 15 mL distilled water. The mixture was placed in a sealed 35 mL borosilicate glass vessel, which was heated in a Discover SP CEM microwave under autogenous pressure and cooled down to room temperature. The as-obtained white power was finally recovered by filtration, and washed with EtOH. For the whole series, the chemical yields were around 40%. The targeted compositions for Tb$_{2-x}$Eu$_x$ was x = 0.02, 0.06, 0.10, 0.20. Anal. Calcd. for Tb$_{1.98}$Eu$_{0.02}$C$_{20}$O$_{22}$H$_{18}$ (%): C, 25.9 ; H, 2.0. Exp : C, 26.0 ; H, 1.6 Anal. Calcd. for Tb$_{1.94}$Eu$_{0.06}$C$_{20}$O$_{22}$H$_{18}$ (%): C, 25.9 ; H, 2.0. Exp : C, 25.9 ; H, 1.7. Anal. Calcd. for Tb$_{1.9}$Eu$_{0.1}$C$_{20}$O$_{22}$H$_{18}$ (%): C, 25.9; H, 2.0. Exp: C, 26.1 ; H, 1.7. Anal. Calcd. for Tb$_{1.8}$Eu$_{0.2}$C$_{20}$O$_{22}$H$_{18}$ (%) : C, 25.9 ; H, 2.0. Exp : C, 25.9 ; H, 1.7.
The Eu and Tb contents (in percentage) were determined by ICP-AES and are reported in Supporting information Table S1.

1.2. Physical characterization

Powder X-ray Diffraction spectra were monitored using a D8 Bruker diffractometer in the Bragg-Brentano geometry, equipped with a front germanium monochromator, a copper anode (CuKα L3 radiation λ=1.540598 Å) and a LynxEye PSD detector.

Single-crystal X-ray Diffraction were performed on a Rigaku Synergy S equipped with a microsource tube with Mo anode (and Montel-type focusing optics), a Hypix6000 hybrid pixel Si detector and a nitrogen cryogenic system (Oxford Cryosystems 800+).

FTIR spectra were recorded in the 4000–400 cm^{-1} range on a Bruker Vertex equipped with a computer control using the OPUS software.

Thermogravimetric analysis (TGA) was performed by flowing dry air with a heating and cooling rate of 5°C/min on a SETARAM TG-DSC 111 between 20 and 800°C.

For ICP-AES analyses, samples were dissolved in a 10% HNO_3 solution and analyzed by ICP-AES. The calibration curve was established from the analysis of five standard solutions containing Eu and Tb in various contents to cover a range in accordance with targeted concentrations. The standard solutions were prepared with high purity monoelemental solutions in acidic solution.

Room-temperature photoluminescence measurements (emission, excitation and lifetimes) were recorded on a Jobin-Yvon Fluorolog 3 fluorimeter equipped with a CCD camera (excitation source: 450 W Xe arc lamp). Emission spectra were corrected for detection and optical spectral response of the spectrofluorimeter and the excitation spectra were weighed for the spectral distribution of the lamp intensity using a photodiode reference detector.

The low temperature measurements were performed on a SPEX FL212 Jobin Yvon spectrofluorometer in a front-face configuration. The excitation spectra were corrected for the variation of the incident flux (450W Xe lamp); the emission spectra were corrected for the transmission of the monochromator as well as the response of the photomultiplier. An excitation/emission double monochromator insure a resolution equal to 2 nm per millimeter of aperture. Slits apertures, increments, and acquisition times were adjusted for optimized signal- to-noise ratio and resolution. A thermoelectrically cooled photomultiplier tube was used. An Oxford cryostat connected to a dynamic pumping system ensures the circulation of helium gas. The temperature was monitored through a thermal probe in direct contact with the copper sample holder. After reaching the targeted temperature, a dwell time of 15 minutes was fixed before launching the emission/excitation acquisition so that to insure the thermal homogeneity of the sample.

2. Results and discussion (Fig. S1 to S17)
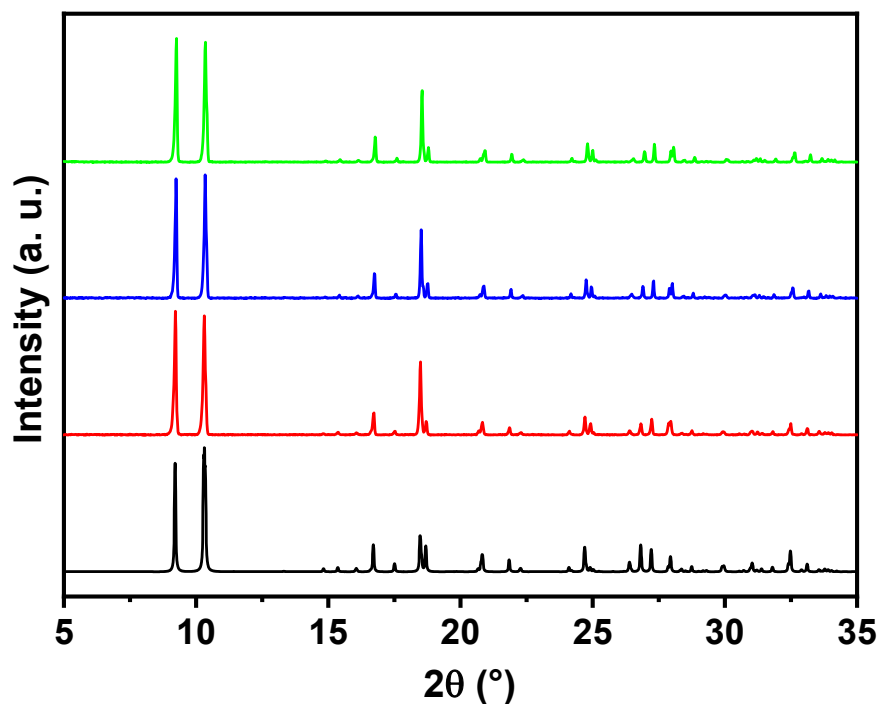
Figure S1. XRD pattern of the compounds **Tb-MOF** (green line), **Eu-MOF** (red line), **Gd-MOF** (blue line) compared to the simulated one from literature.[1]
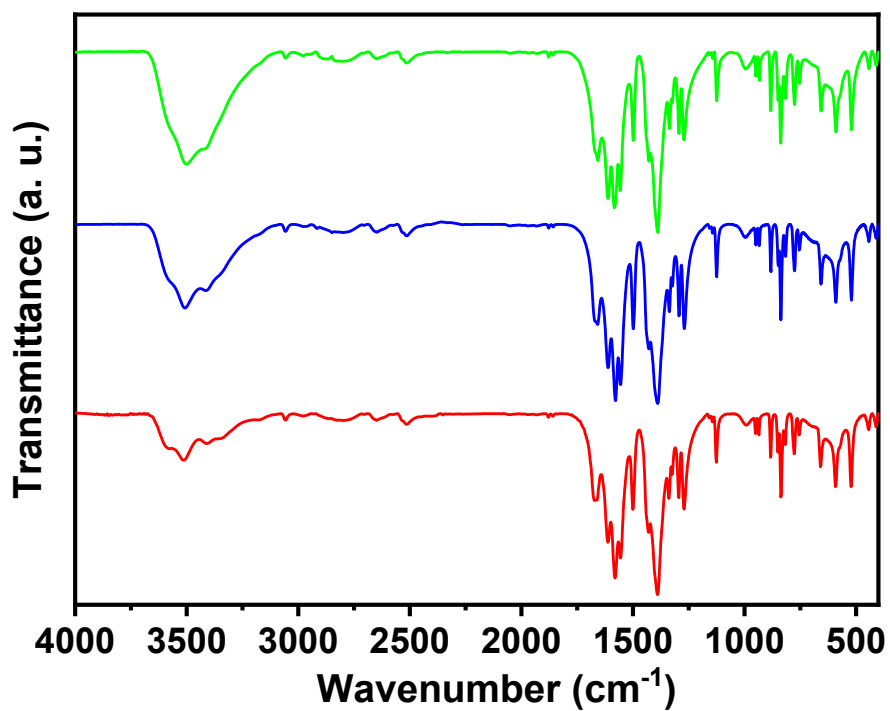
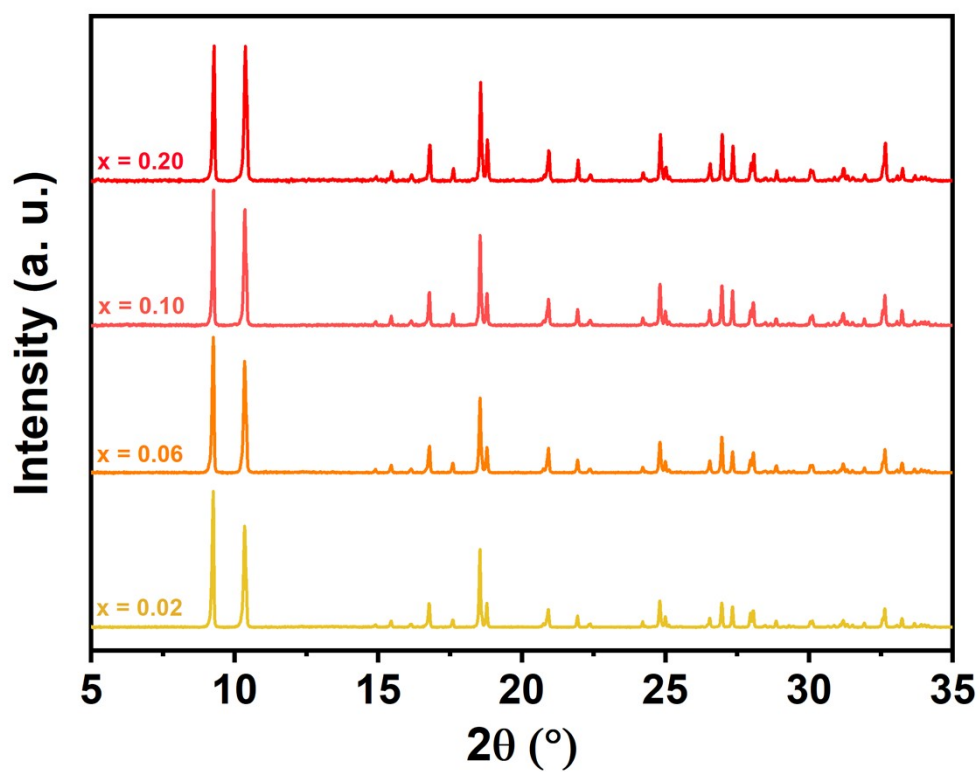**Figure S2.** FT-IR spectra of the compounds **Tb-MOF** (green line), **Eu-MOF** (red line), **Gd-MOF** (blue line).

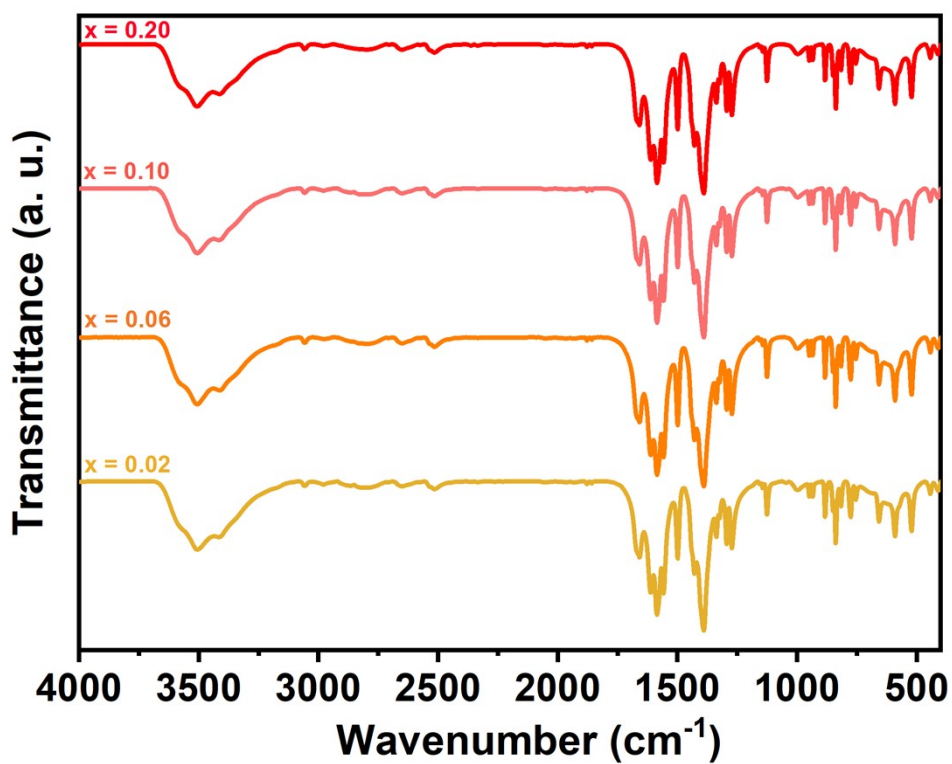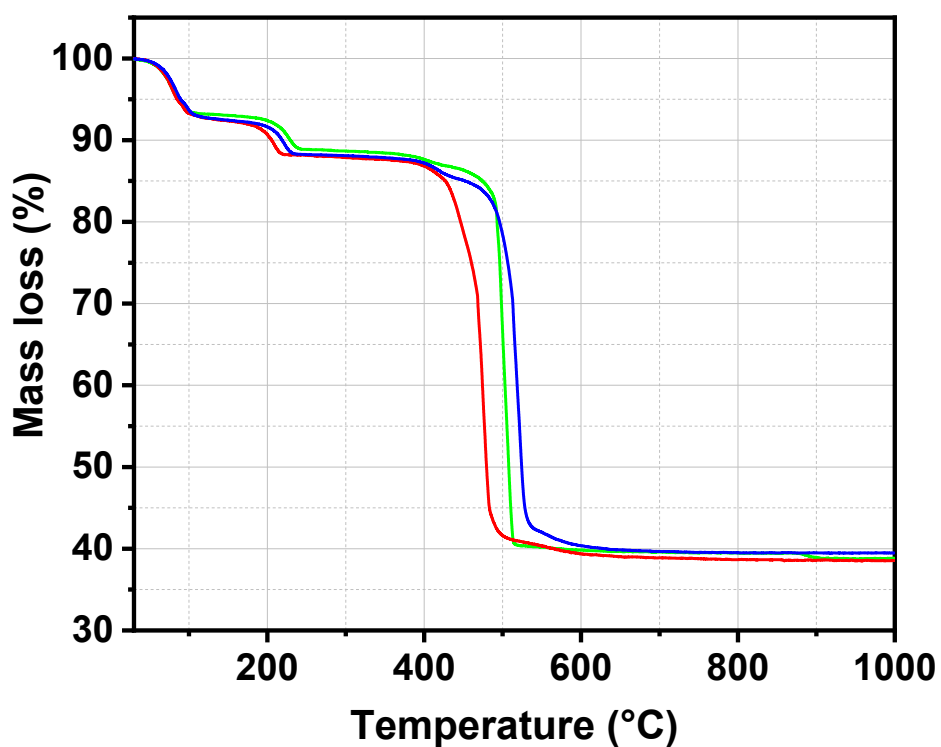**Figure S3**. XRD pattern of the compounds **Tb$_{2-x}$Eu$_x$-MOF** with x =0.02, 0.06, 0.10, and 0.20.

Figure S4. FT-IR spectra of the compounds **Tb$_{2-x}$Eu$_x$-MOF** with x =0.02, 0.06, 0.10, and 0.20.

Figure S5. : Thermal analyses of the compounds **Tb-MOF** (green line), **Eu-MOF** (red line), **Gd-MOF** (blue line).
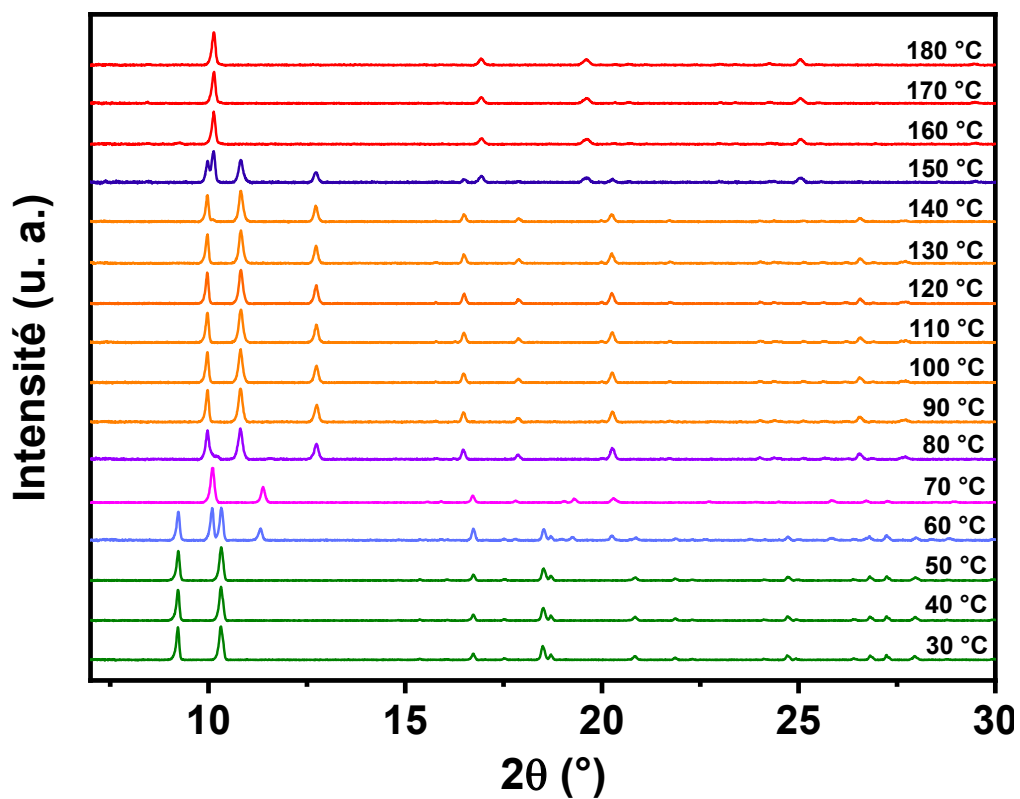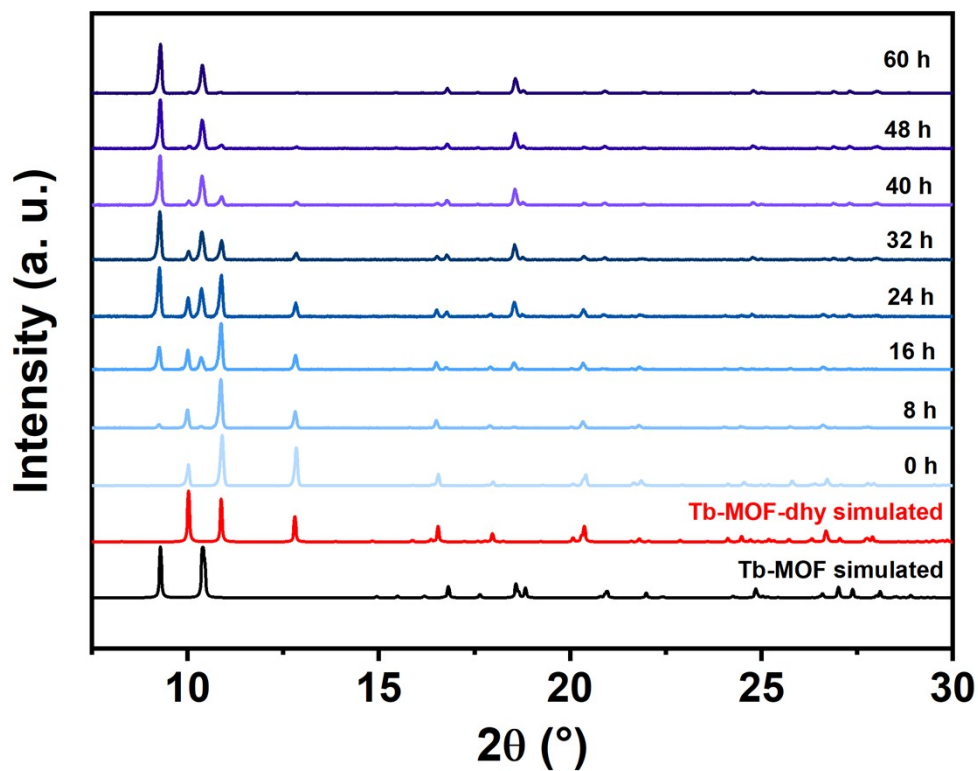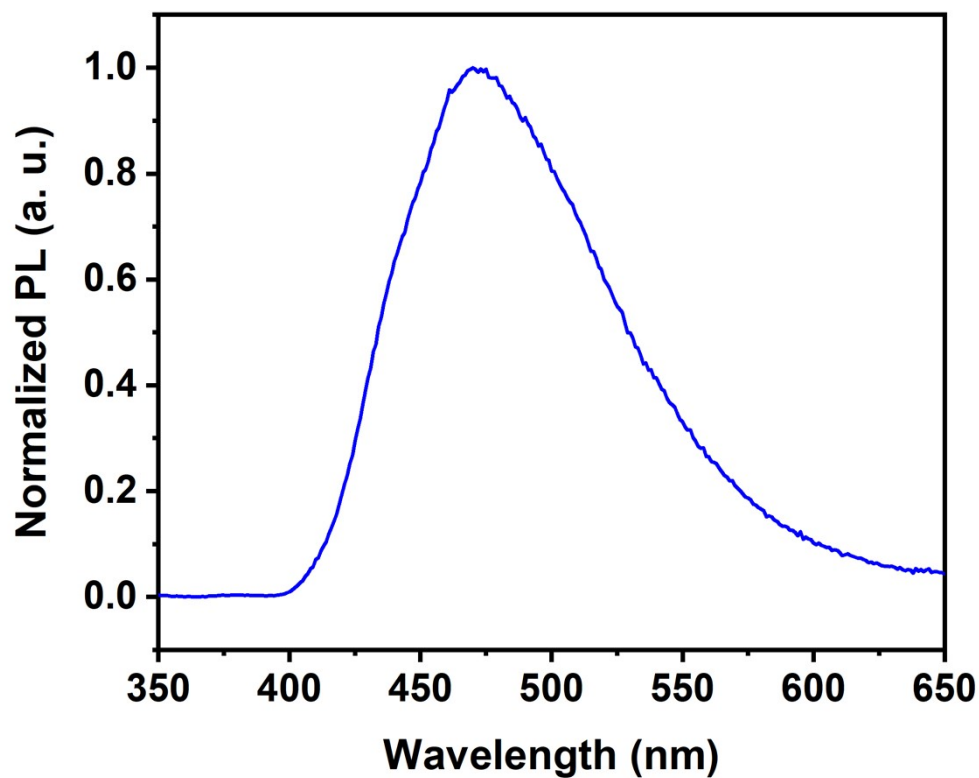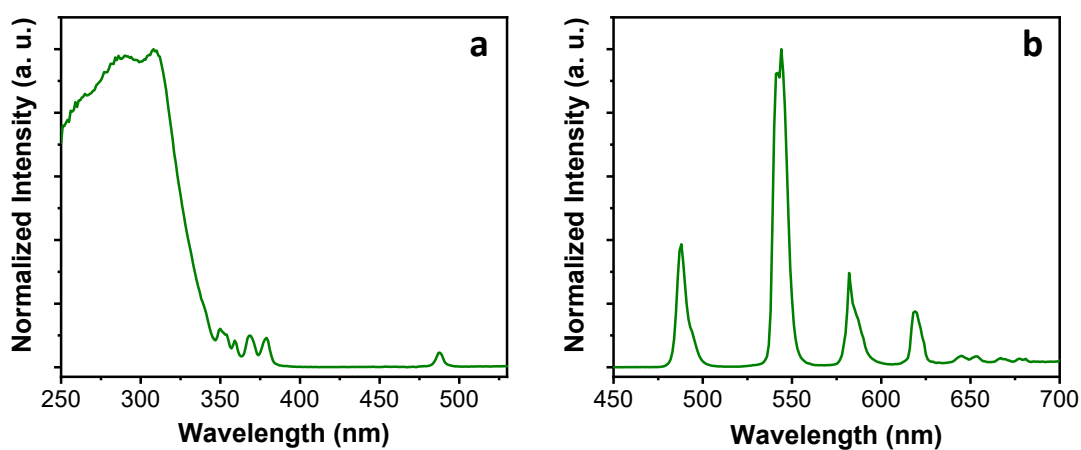

Figure S6. X-ray thermodiffractogram of **Tb-MOF** performed under air from 30°C to 180°C using a 10°C step.
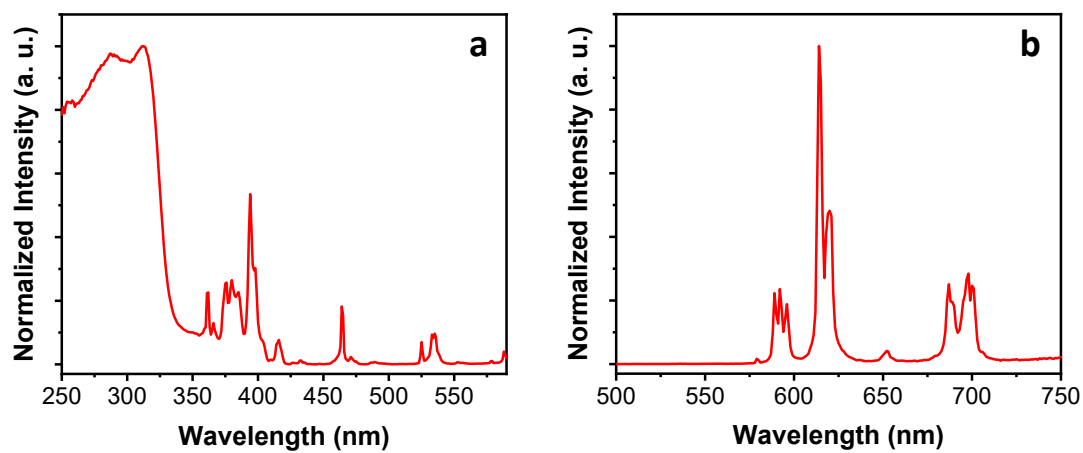
Figure S7. Room temperature powder X-ray diffraction pattern of **Tb-MOF-dhy** after various air exposition time, from 0 to 60 h after its complete dehydration.

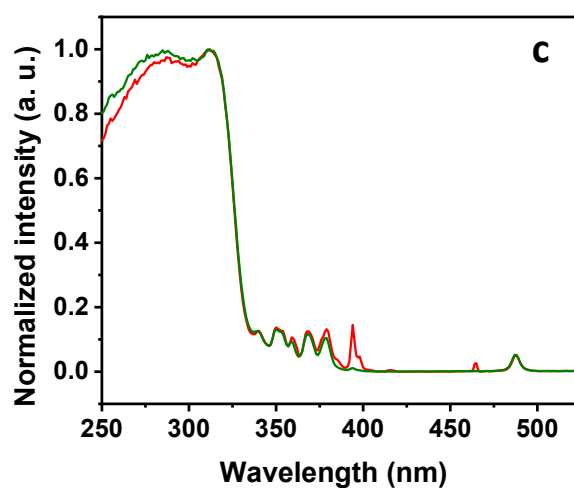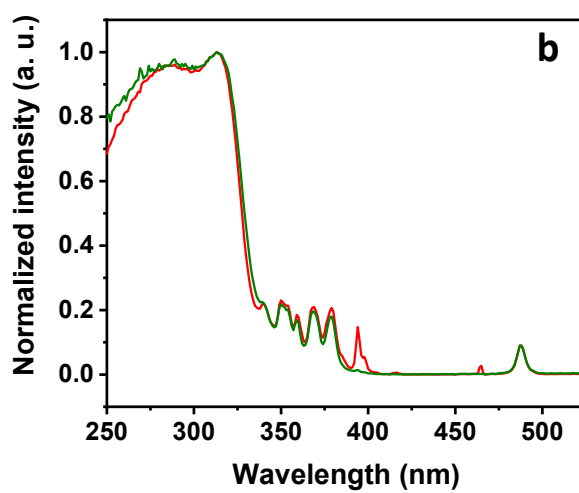**Figure S8.** Phosphorescence spectrum at 77K of **Gd-MOF** excited at 309 nm.
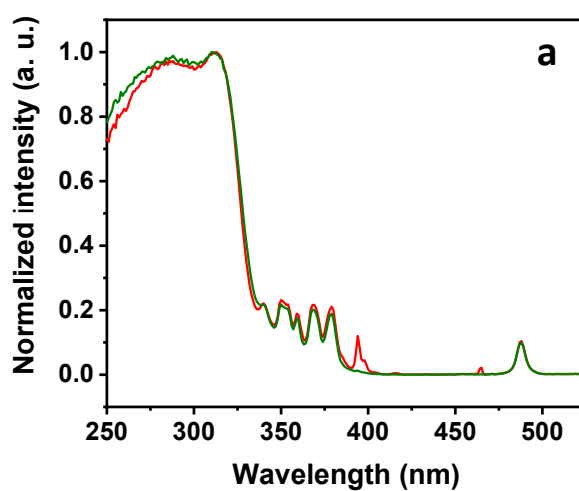
Figure S9. (a) Excitation spectrum monitoring the emission at 544 nm, and **(b)** emission spectrum exciting at 309 nm of **Tb-MOF**.
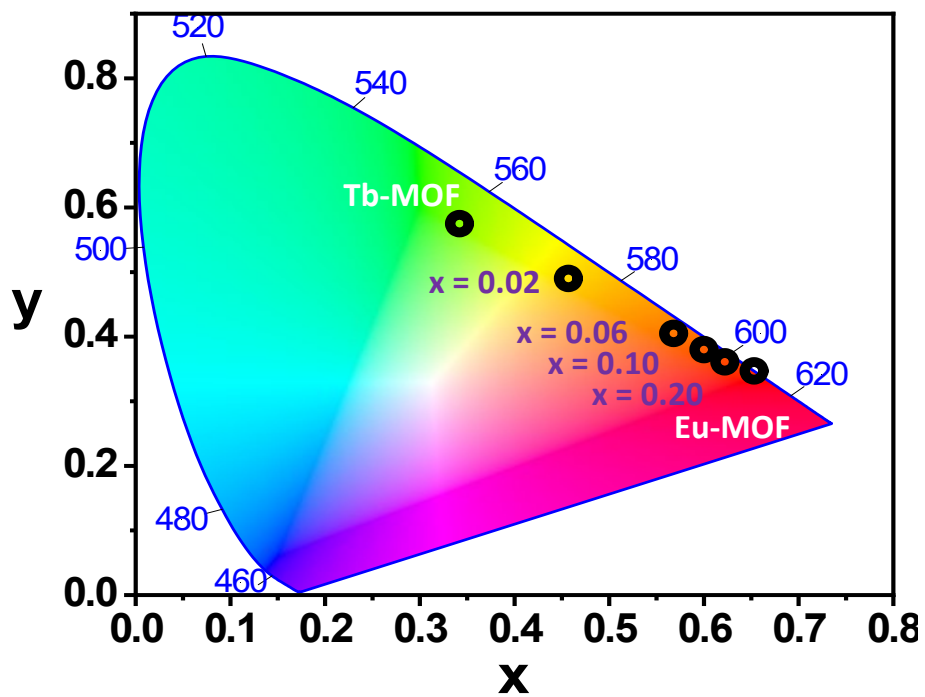

Figure S10. (a) Excitation spectrum monitoring the emission at 614 nm, and **(b)** emission spectrum exciting at 309 nm of **Eu-MOF**.
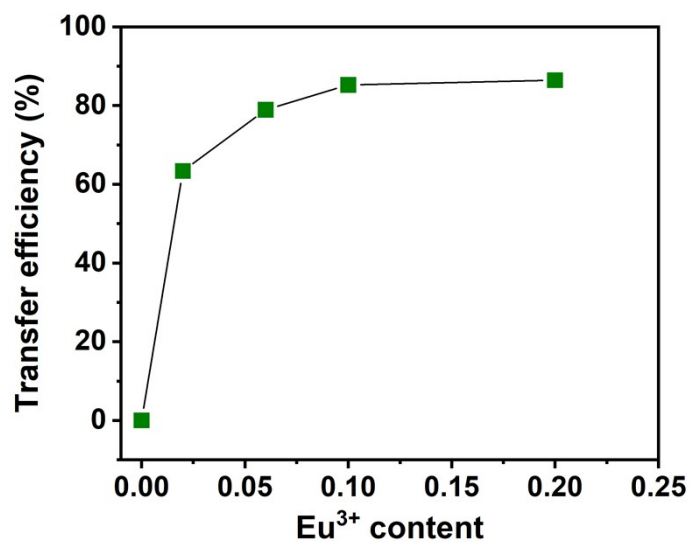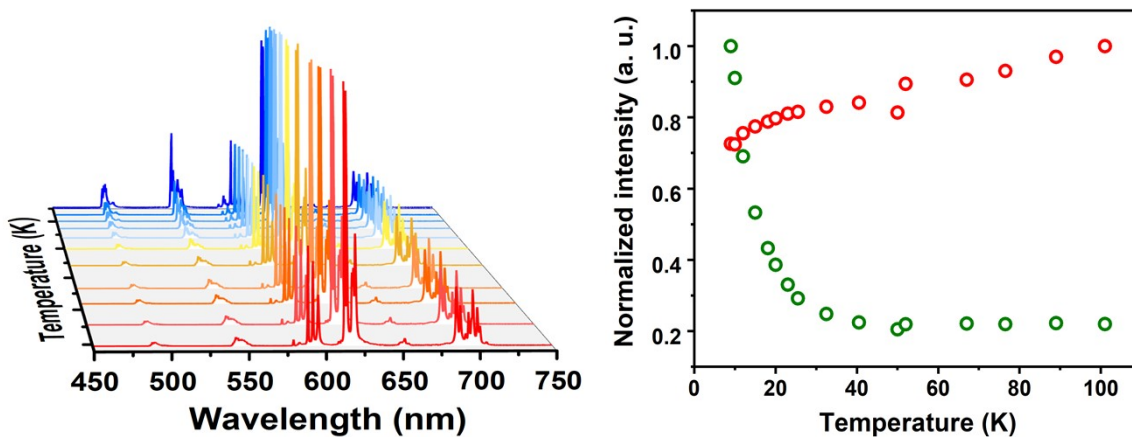
Figure S11. Room temperature excitation spectra of monitoring at 614 nm ($^5D_0 \rightarrow {}^7F_2$ transition of Eu^{3+}, red line) and at 544 nm ($^5D_4 \rightarrow {}^7F_5$ transition of Tb^{3+}, green line) of a) **$Tb_{1.94}Eu_{0.06}$-MOF**, b) **$Tb_{1.90}Eu_{0.10}$-MOF**, and c) **$Tb_{1.80}Eu_{0.20}$-MOF.**

Figure S12. CIE chromaticity diagram of the **Tb$_{2-x}$Eu$_x$-MOF** samples calculated from the emission spectra at room temperature under 309 nm excitation.


Figure S13. Tb^{3+}-to-Eu^{3+} energy transfer efficiency of **Tb$_{2-x}$Eu$_x$-MOF** samples calculated from the lifetimes of the $^5D_4$ level after excitation at 309 nm.

Figure S14. Temperature-dependent emission spectra in the 10-100K range for upon 309 nm excitation of **Tb$_{1.80}$Eu$_{0.20}$-MOF** and corresponding dependence of the normalized integrated area of I$_{Tb}$ (green points) and I$_{Eu}$ (red points).
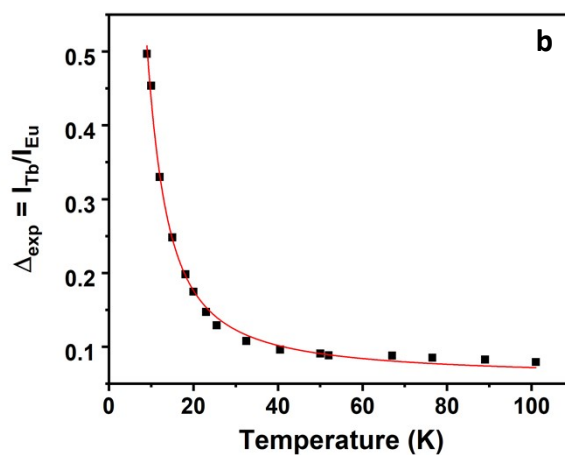
Figure S15. Temperature-dependence of the thermometric parameter Δ in the 10-100K range for the compound **Tb$_{1.80}$Eu$_{0.20}$-MOF** excited at 309 nm. The red lines represent the calibration cruve obtained from the best fit of experimental points according the Mott-Seitz equation.
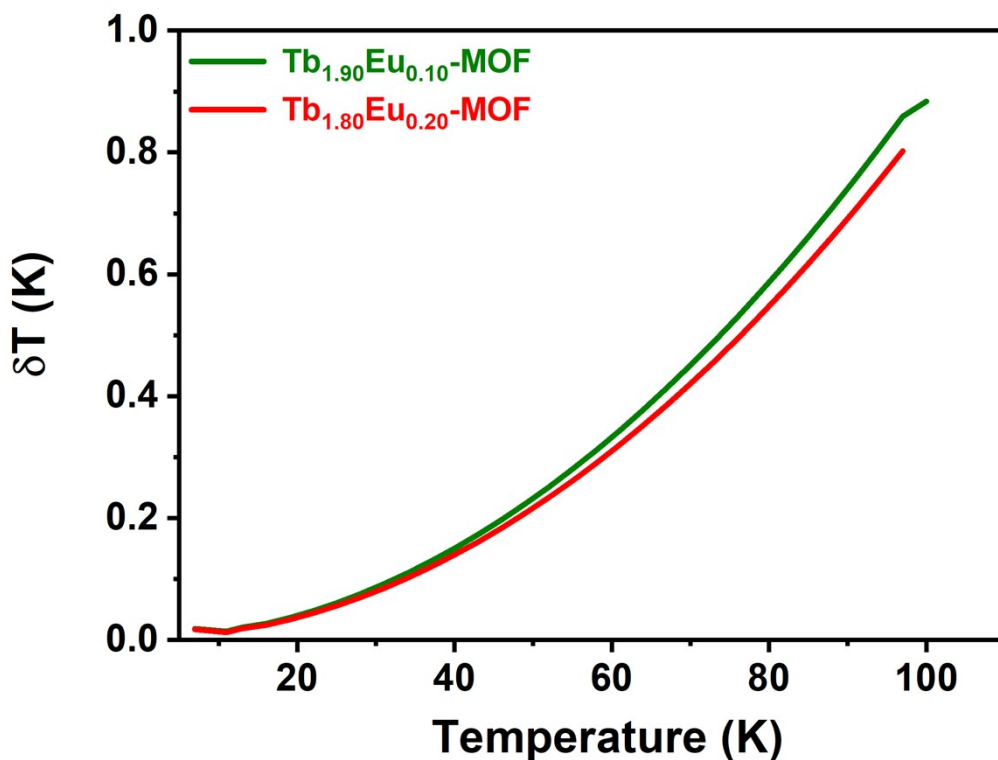
Figure S16. Temperature uncertainty ($\delta T = {}^1\!/S_r \times \delta\Delta/\Delta$), in the $10 - 100$ K range ($\delta\Delta/\Delta$ was estimated as 0.2% for a photomultiplier) for the compounds **Tb$_{1.90}$Eu$_{0.10}$-MOF**, and **Tb$_{1.80}$Eu$_{0.20}$-MOF**.
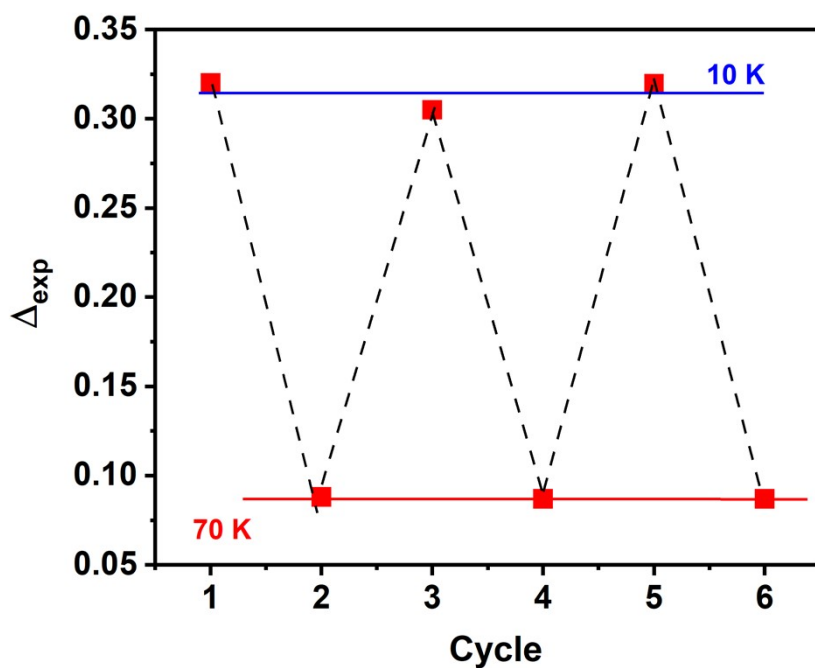
Figure S17. Temperature cycling between 10 and 70 K revealing a repeatability > 99% for the **Tb$_{1.80}$Eu$_{0.20}$-MOF** compound.

Table S1. ICP composition of the compounds **Tb$_{2-x}$Eu$_x$-MOF** with x =0.02, 0.06, 0.10, and 0.20.

Theoretical composition	Experimental composition
Tb$_{1.980}$Eu$_{0.020}$-MOF	Tb$_{1.981}$Eu$_{0.019}$
Tb$_{1.940}$Eu$_{0.060}$-MOF	Tb$_{1.931}$Eu$_{0.069}$
Tb$_{1.900}$Eu$_{0.100}$-MOF	Tb$_{1.881}$Eu$_{0.119}$
Tb$_{1.800}$Eu$_{0.200}$-MOF	Tb$_{1.771}$Eu$_{0.229}$

Table S2. Crystallographic data of **Tb-MOF-dhy**.

	Tb-MOF-2-dhy
Empirical formula	Tb$_2$C$_{20}$O$_{18}$H$_{10}$
Formula weight (g/mol)	847.04
Temperature (K)	373.15
Crystal system	Monoclinic
Space group	$P2_1$/n
a/Å	16.8704(7)
b/ Å	7.2155(2)
c/ Å	18.3095(5)
α/°	90
β/°	104.552(4)
γ/°	90
Volume/ Å^3	2157.29(13)
Z	4
ρ_{calc} (g/cm^3)	2.605
Data/parameters	5349/361
R$_{int}$	0.1563
wR$_2$ (I>=2σ (I))	0.1999
R$_1$ (all data)	0.0906
wR$_2$ (all data)	0.2282

Table S3. Chromaticity coordinates of compounds **Tb$_{2-x}$Eu$_x$-MOF** with x = 0 (**Tb-MOF**), 0.02, 0.06, 0.10, 0.20, and 2 (**Eu-MOF**) excited at 309 nm.

Compound	(x;y) coordinates
Tb-MOF	(0.342 ; 0.575)
Tb$_{1.980}$Eu$_{0.020}$-MOF	(0.457 ; 0.490)
Tb$_{1.940}$Eu$_{0.060}$-MOF	(0.568 ; 0.405)
Tb$_{1.900}$Eu$_{0.100}$-MOF	(0.600 ; 0.380)
Tb$_{1.800}$Eu$_{0.200}$-MOF	(0.622 ; 0.361)
Eu-MOF	(0.653 ; 0.347)

Table S4. Room temperature lifetimes of $^5D_4$ (Tb^{3+}) and $^5D_0$ (Eu^{3+}) obtained from the decay curve fitting with a single exponential model, and Tb^{3+}-to-Eu^{3+} energy transfer efficiency.

Compound	$^5D_4$ (μs)	$^5D_0$ (μs)	η_{ET} (%)
Tb-MOF	1434 ± 9		
$Tb_{1.98}Eu_{0.02}$-MOF	525 ± 3	757 ± 9	63.4
$Tb_{1.94}Eu_{0.06}$-MOF	302 ± 4	608 ± 5	78.9
$Tb_{1.90}Eu_{0.10}$-MOF	211 ± 6	577 ± 4	85.3
$Tb_{1.80}Eu_{0.20}$-MOF	194 ± 4	543 ± 1	86.4
Eu-MOF		524 ± 2	

References:

[1] R. Cao, D. Sun, Y. Liang, M. Hong, K. Tatsumi and Q. Shi, *Inorg. Chem.*, 2002, **41**, 2087–2094.